Research on Engineering Structures & Materials
www.jresm.org
Research Group

Research Article

Energy absorption reparability of PLA Body-Centered Cubic (BCC) lattice structure considering manufacturing defects

Mario Soldo *,a

Faculty of Mechanical Engineering, Computing and Electrical Engineering, University of Mostar, Bosnia and Herzegovina

Article Info

Article History:

Received 23 Jun 2026

Accepted 28 Sep 2026

Keywords:

Lattice structures;
Body-Centered Cubic (BCC);
Relative density;
Additive manufacturing;
FFF;
Energy absorption capacity

Abstract

This paper investigates repeatability of additive manufacturing on the energy absorption capacity of polymer Body-Centered Cubic (BCC) lattice structures. As a class of cellular materials, lattice structures enable the tailoring of macroscopic properties through controlled microgeometry, where relative density, unit cell topology, print quality and manufacturing defects play a significant role. BCC lattice structures with a relative density of approximately 0.2 were designed in Rhinoceros using Grasshopper plugin and fabricated using fused filament fabrication (FFF) technology with PLA material. Experimental compression tests were conducted to evaluate the force – displacement response and determine the energy absorption characteristics of the structures. The results showed that lattice structures with uniform spatial distribution of BCC unit cells achieved an average peak force of 2529.89 N at an average compression displacement of 4.04 mm. Although manufacturing defects did not significantly affect the maximum load-bearing capacity, it strongly influenced the deformation behavior of the lattice structures. After reaching the peak load, diagonal collapse of the structures was observed, indicating limited post-elastic energy absorption capability. The average specific energy absorption of the tested structures was 0.41 J/g, with a coefficient variation of 11.32%. The results demonstrate that manufacturing defects contribute to the variability in energy absorption of FFF-fabricated BCC lattice structures. Their mechanical influence is governed not only by defect number but also by defect type relative to load-bearing struts and nodes. These findings highlight the importance of defects caused by FFF production in usable products for achieving favorable energy absorption characteristics.

© 2026 MIM Research Group. All rights reserved.

1. Introduction

Lattice structures, included in cellular structures along with honeycomb and foam structures, are defined as three-dimensional porous spatial structures formed by unit cells with different topological geometries that are spatially tessellated. Through careful design of the microgeometry of lattice structures, precise tailoring of their macroscopic properties is enabled. The main characteristics that influence the mechanical properties of lattice structures at the macro level are: unit cell topology (determined by the nodal connectivity of struts), unit cell morphology (characterized by the shape and geometry of struts and nodes), lattice structure morphology (defined by the spatial distribution and orientation of unit cells), relative density of the lattice structure and mechanical properties of the building material [1]. Relative density of the lattice structure $\overline{\rho}$ is defined as the ratio of the density of the porous structure ρ and the density of the constituent ρ_S. It is also equivalent to the volume fraction of the porous structure relative to the solid structure [2]. Relative density is closely related to stiffness, i.e. as the relative density of the lattice structure increases, the stiffness of the structure itself also increases [3]. When the building

*Corresponding author: mario.soldo@fsre.sum.ba
[a]orcid.org/ 0009-0005-8499-6494
DOI: http://dx.doi.org/10.17515/resm2026-1783me0623rs

material and relative density are constant, the mechanical properties of lattice structures depend on the architecture of the unit cells of the lattice structure [4] and on manufacturing defects. Lattice structures obtained through additive manufacturing have found wide application in automotive production (as crash absorbers) made of nylon with carbon fibres [5], in personal protective use such as pads made personalized for the user [6] up to application in the sports shoe's soles, car tires and in the interior of a modern helmet [7]. Regarding the impact of additive manufacturing on the mechanical properties of lattice structures, Banaszek et al. [8] experimentally and numerically investigate compressive behaviors of PETG BCC lattice structures fabricated by FFF additive manufacturing, concluding that the mechanical response significantly depends on the orientation during printing, but also on the loading conditions and strut modelling parameters. Kumar et al. [9] experimentally and numerically investigate a new shell-like lattice structure fabricated by FDM process, concluding that such a geometry enables unsupported printing with a significant printing time reduction and material consumption reduction, while simultaneously achieving approximately twice the stiffness and energy absorption compared to a BCC lattice structure of equal relative density.

One of the most researched unit cell topologies, next to Simple Cubic (SC), is certainly the Body-Centered Cubic (BCC) unit topology, which stands out for its simple but extremely functional architecture. BCC lattice structures consist of a cubic arrangement where a node in the center of gravity of the cube is connected to all eight corners, such a pattern is repeated in a three-dimensional grid. Azmi et al. [10] investigate the influence of strut diameter on the static and dynamic behavior of BCC lattice structures made of ABS material using the FDM printing process and concludes that a larger strut diameter increases the total moment of inertia, which leads to greater stiffness and higher natural frequencies. Distefano et al. [11] numerically and experimentally investigate the mechanical and morphological properties of two types of 3D periodic lattice structures based on the BCC unit cell (a strut-assembled structure called G7 and a TPMS-derived structure called IWP) and conclude that the G7 structure requires improvement in compression test behaviors, while the IWP structure exhibits a gradual, controlled collapse, and decreasing the unit cell diameter improves the performance of both structures. Dong et al. [12] investigate the reinforcement of sustainable building materials with 3D printed polymer BCC lattice structures to improve their flexural mechanical properties. They conclude that the incorporation of polymer lattices significantly increases the flexural strength and ductility of the composites. The specific energy absorption (SEA) is an important performance metric for lattice structures, representing the amount of energy absorbed during mechanical deformation per unit mass of the structure. This parameter is particularly important in the analysis of porous and lattice structures produced by additive technologies, as it allows for a comparison of the efficiency of different geometries regardless of their dimensions and a more detailed explanation of manufacturing defects of the same test specimens. The total absorbed energy is determined as the area under the force – displacement curve obtained from a compression test:

$$EA = \int_0^{\delta_{max}} F(\delta)\, d\delta \tag{1}$$

where: EA – total absorbed energy (J), δ_{max} – total global displacement (mm) and $F(\delta)$ – impact force during compression (N). δ_{max} refers to the maximum displacement that the lattice structure can withstand during the compression test before structural fracture or lattice densification. However, the total absorbed energy alone is not sufficient for an objective comparison of test specimens, since larger specimens can naturally absorb a greater amount of energy due to their larger mass. Therefore, the specific energy absorption capacity is introduced, which represents the ratio of the total absorbed energy to the mass of the test specimen:

$$SEA = \frac{EA}{m} \tag{2}$$

where: SEA – specific energy absorption per specimen mass (J/g), EA – total absorbed energy (J) and m – sample mass (g). Physically, this parameter describes the efficiency of the structure in absorbing energy. High values of specific energy absorption are especially important in applications such as impact protection, automotive energy absorbers, biomechanical implants,

aerospace structures and protective equipment and packaging systems. For lattice structures manufactured by FFF technology, the ability to absorb energy per mass unit is one of the key criteria for evaluating mechanical performance, but the results can also be used to assess the consistency of individual specimens manufactured using FFF technology. Regarding the testing of the energy absorption ability of lattice structures, Yu et al. [13] investigate the development and effectiveness of different types of grid structures for energy absorption and shock loads and conclude that advanced structures such as TPMS, bio-inspired and gradient grid structures show very high performance, although improvements in design, proper choice of materials and higher production precision are still need to investigated for their wider application. Xu et al. [14] investigated the influence of the type of thermoplastic material and the printing orientation on the mechanical properties and energy absorption capacity of different TPMS lattice structures, and they concluded that PLA material provides the highest specific energy absorption.

This study investigates the specific energy absorption capacity of BCC lattice structures with a defined relative density, fabricated from PLA using FFF additive manufacturing with particular emphasis on the influence of manufacturing defects on energy absorption performance. The effect of process-induced defects on the repeatability and consistency of energy absorption is also examined. A qualitative interpretation of the observed mechanical response is provided to facilitate a detailed understanding of the relationship between manufacturing imperfections and energy absorption behavior. In addition, the methodology adopted in the study, including lattice structure modelling, additive manufacturing, compression testing and validation of the experimental results, is described in sufficient detail to support the reproducibility of similar investigations in future research.

2. Research Methodology

Fig. 1 illustrates the methodology used in this study. In the first step of the presented methodology, a unit cell topology is defined.

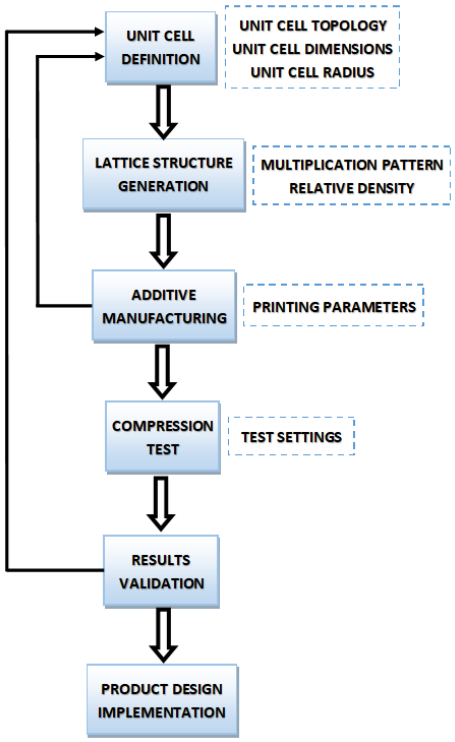


Fig. 1. Research methodology

There are many different unit cell topologies as stated at [15], but the boundary between the original and derived unit cell topologies is still not clearly defined. A very useful creation in topology selection, which results in predicting the mechanical behavior of 3D lattice structures under compression, was introduced by Maxwell using the expression:

$$M = b - 3j + 6 \tag{3}$$

where: b – number of struts and j – number of nodes. Depending on the sign of M, the mechanical response of the lattice structures is predicted to be either bending-dominated or stretching-dominated. A negative value of M indicates structures with bending-dominated behaviour, while a positive value (or a value equal to zero) characterizes structures with stretching-dominated behaviour. The stress – strain diagram for structures with bending-dominated and stretching-dominated behavior is shown in Fig. 2. Eq. (3) is often used as a guideline for choosing a topology with respect to the expected compression response [16]. However, it is not good to use only Maxwell criterion for predicting the behavior of lattice structures, since the cross-section of the unit cell, the building material or the defects of the manufactured lattice structures are not considered. Within this first initial step, the dimensions of the unit cell and the radius of the struts are also selected. The dimensions should be selected depending on the selected type of additive manufacturing of the lattice structure, since small unit cells may not be successfully manufactured. In the second phase, the pattern of multiplication of the unit cells is selected. The multiplication pattern defines the final volume of the lattice structure. This is followed by the additive manufacturing step. The additive manufacturing process consists of defining the position of the lattice structures within the printer working volume, material selection, the orientation of the test samples and the printing parameters. The final stages are compression testing, validation of results (quantitative and intuitive) and, if the results meet expectations, implementation into the product design. If the obtained results do not demonstrate a satisfactory response, it is always possible to return to one of the previous steps, therefore, the presented methodology can be considered as iterative process.

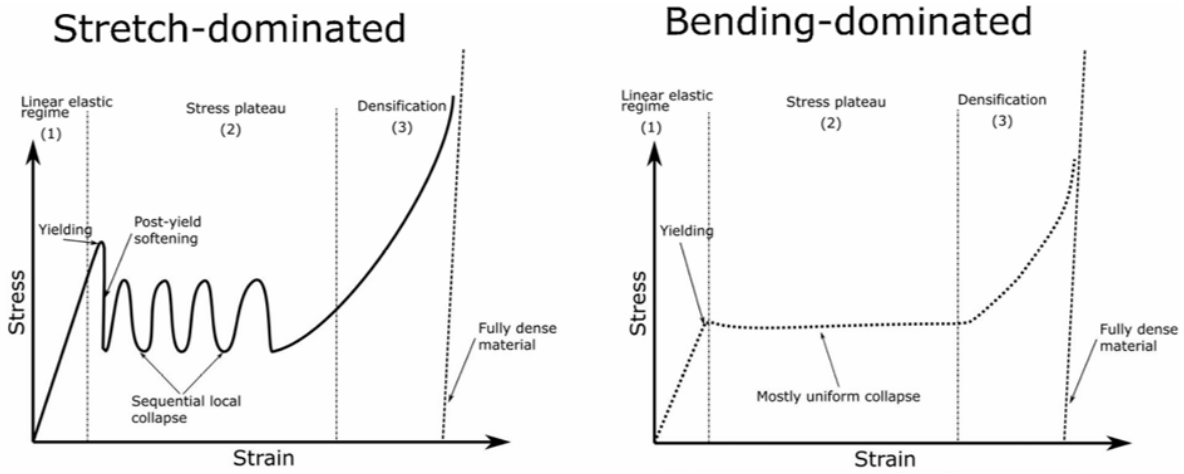


Fig. 2. Compression behavior described by stress – strain diagrams for structures with stretching-dominated (left) and bending-dominated (right) behavior

3. Unit Cell Lattice Structure Generation

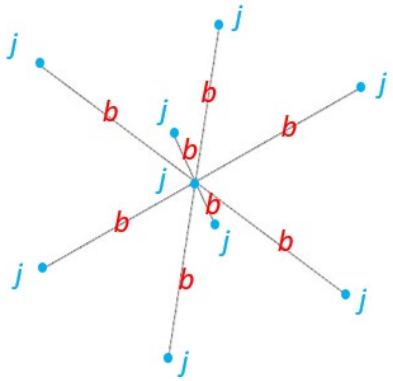


Fig. 3. Body-Centered Cubic (BCC) unit cell with marked 8 supports (b) and 9 nodes (j)

For this study, the Body-Centered Cubic (BCC) unit cell topology was chosen. The BCC unit cell topology, whose wireframe representation is shown in Fig. 3, has a negative Maxwell value (for eq. (3) $M = -13$) which suggests that the lattice structure exhibits bending-dominated behavior under compression. A wireframe model of the BCC unit cell is defined in Rhinoceros program with the dimensions of 10 mm x 10 mm x 10 mm. The selected dimensions are adjusted, assuming successful FFF additive manufacturing. With the Grasshopper plugin, the MultiPipe command is defined (as shown in Fig. 4) to add radius to the struts.

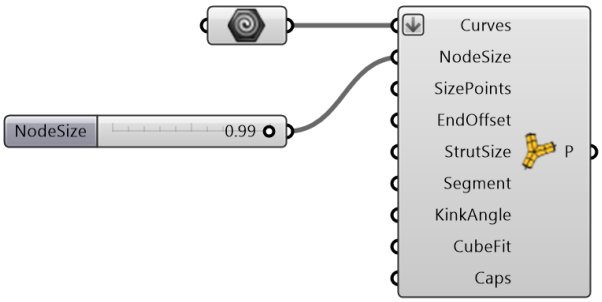


Fig. 4. MultiPipe command settings in Grasshopper plugin in Rhinoceros program

A radius of 0.99 mm is selected to define the NodeSize, with the Flatten subcommand activated in the Curves command and round defined in the Caps command, so that the unit cell behaves as unity and has closed and rounded edges. It is important to emphasize that the NodeSize radius initiates the strut diameter. For this research, NoseSize radius was selected depending on the selected relative density. Since the dimensions of the unit cell exceed the defined volume, after the Bake command, the strut extensions are cut, as shown on Fig. 5.

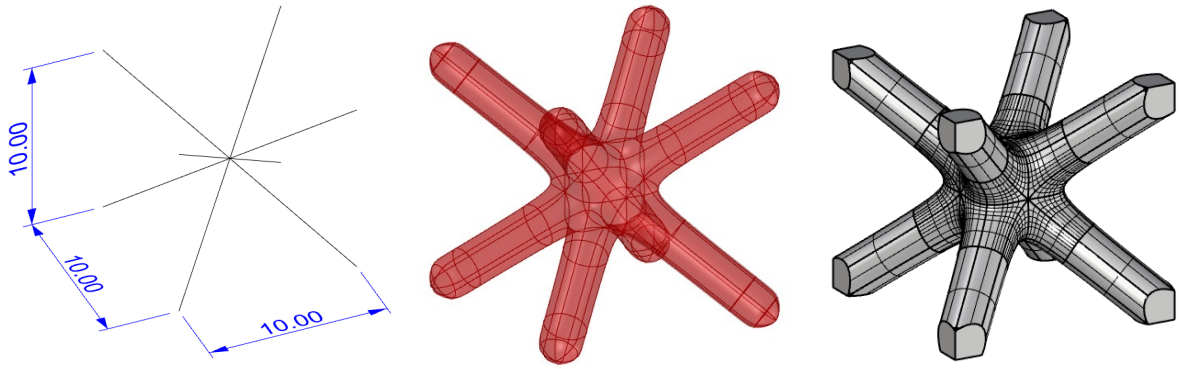


Fig. 5. Wireframe dimensions of BCC unit cell (left), Grasshopper result after adding MultiPipe command (middle) and completed BCC unit cell after cutting (right)

4. Lattice Structure Modelling

After defining the unit cell topology within the chosen dimensions, the pattern of unit cell multiplication is defined. The best evidence of the diversity of unit cell dimensions and the pattern of unit cell multiplication in lattice structures was shown by Khiavi et al. [18] who summarized several studies of different unit cell topologies (SC, BCC, Kelvin, Circular, Octahedron, Octagonal…) of different polymer materials (PLA, ABS, PA12, PA1102…) obtained by different types of additive technology (FDM, SLS, MJF, SLA…). The paper states that the unit cells are multiplied by a repeating (3 x 3 x 3 – 8 x 8 x 8) or variable (5 x 5 x 4, 4 x 4 x 3, 4 x 4 x 8, 10 x 10 x 4 …) multiplication pattern. For the purposes of research, a 5 x 5 x 5 repeating pattern of the BCC unit cell was selected, resulting in a lattice structure embedded within a cubic volume of 50 mm x 50 mm x 50 mm. For the analysis of the compression properties of lattice structures, a relative density of 0.2 was selected, which indicates 80% porosity of the lattice structure. The selected relative density of 0.2 is due to the possibility of printing such lattice structures, since a lower relative density means a thinner unit cell radius, which is very difficult to print correctly using layer-by-layer material extrusion

technology without major errors and structural defects. Reducing the radius reduces the stiffness and load-bearing capacity of the lattice structure. A higher relative density (e.g. 0.5 or 0.6) indicates lower porosity and thus the radius of the lattice structure would be larger and the unit cell would lose its recognizable shape. Although increasing the radius would increase the stiffness and load-bearing capacity of the lattice structure, it would violate porosity as a basic feature of airy and lightweight lattice structures and the structure could be considered solid with some pores in it. Dividing the volume of the resulting lattice structure modelled in Rhinoceros (25179.575 mm^3) by the volume of the enclosing cube (125000 mm^3) yields a relative density of 0.2014, corresponding to an approximate porosity of 80%.

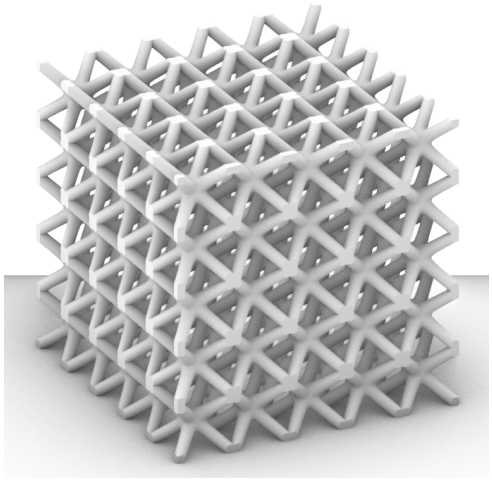


Fig. 6. BCC lattice structure with 0.2 relative density (Rendered model)

The lattice structure is first converted into a single, unified solid using the Bake command in Rhinoceros. Subsequently, all unit cells are merged into a single structure using the Boolean Union operation. The resulting BCC lattice structure (Fig. 6) is then exported in STL format using the Export Selected command and imported into the appropriate slicer software for the selected additive manufacturing printer.

5. Lattice Structure Additive Manufacturing

The 3D printing of lattice structures was performed on a Zortrax M200 Plus printer, using the corresponding software package for model preparation. The selected device is based on FFF (Fused Filament Fabrication) technology, in which the model is formed by melting the material and applying it layer by layer through a heated nozzle onto a heated work platform, as shown on Fig. 7.

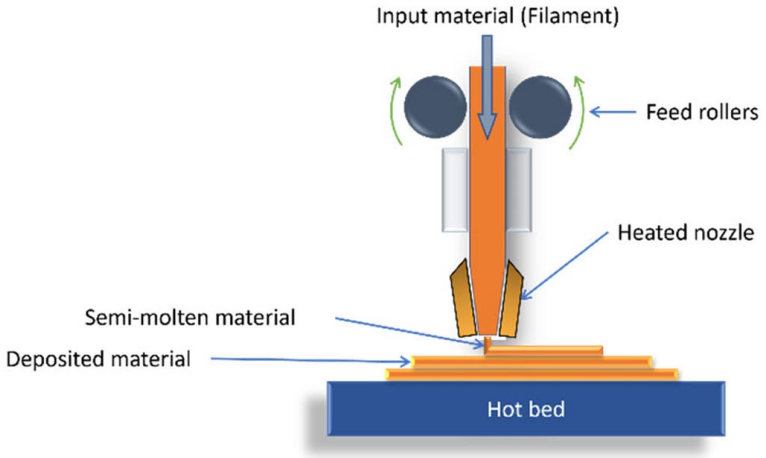


Fig. 7. The FFF process of applying melted material layer by layer on heated platform [19]

The working volume of the closed printing space is 200 mm x 200 mm x 180 mm, while the nozzle diameter is 0.4 mm. Z-Suite software was used to prepare the model for the printing process. As part of this procedure, key process parameters were defined, including device selection, model orientation and positioning in the workspace, selection of build material, generation of support structures, nozzle diameter, layer height, type and pattern of infill, infill density, and temperatures of the work platform and nozzle. PLA (polylactic acid) build material was selected and the most important printing settings are shown in Table 1. PLA material was chosen for its simplicity and reliability of printing, good print quality and lower toxicity of exhaust gases since it is obtained from renewable sources (corn starch or sugar cane). The printing time of one series with four test samples (according to [20], [21]) is 1 day, 14 hours and 10 minutes and the total material consumption is 152 g.

Table 1. Main printing parameters settings

Selected FFF printer type	Selected material	Nozzle diameter (mm)	Infill (%)	Nozzle temp. (°C)	Platform temp. (°C)	Layer (mm)	Print quality
Zortrax M200 Plus	PLA (polylactic acid)	0.4	100 (Solid)	210	60	0.19	Default

6. Compression Testing of Lattice Structures

Compression testing of lattice structures was carried out on a Shimadzu AGS-X universal material properties testing machine with a capacity of 100 kN, which is supported by the computer program Trapezium X. For compression testing of rigid plastic lattice structures, a test speed of 5 mm/min was selected. Since small irregularities are possible during the additive manufacturing of lattice structures (the height of the test sample is 50 mm), a distance between the compression plates of 51 mm is defined so that the samples can be successfully positioned. In the Trapezium-X program, a pre-loading option (so-called Pre-Test) is added, which is carried out in the way of traverse movement in the form of free travel at a defined speed of 5 mm/min. When the compression plate touches the upper surface of the test specimen and a force of 5 N is achieved, the experiment officially begins. The compression test was terminated either when the lattice structure reached 60% compressive deformation (30 mm displacement) or upon sudden failure of lattice structure, whichever occurred first. The resulting force – displacement data were subsequently used to calculate the energy absorption and specific energy absorption according to Eqs. (1) and (2). The output of the compression test is a force – displacement diagram (show in Fig. 8).

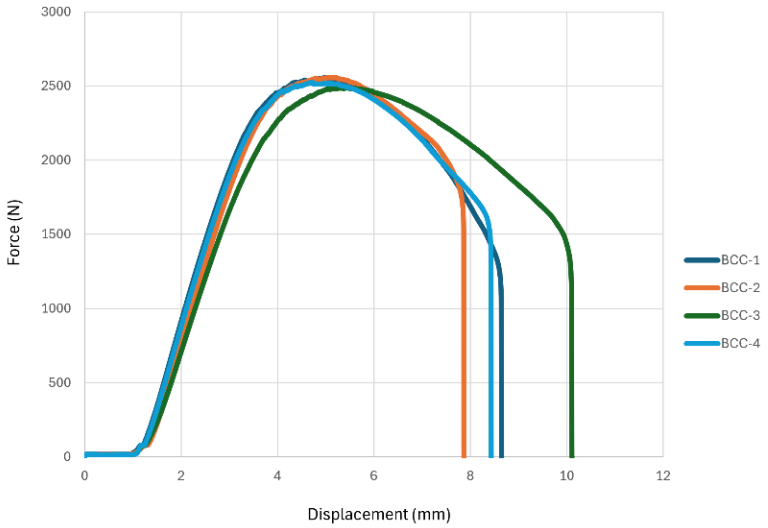


Fig. 8. Force – displacement diagrams of lattice structure samples

Table 2 lists the values of maximum forces (which the specimens experience immediately before the first significant fracture within the lattice structure), displacement values when the maximum force occurs and total displacement. The reported values for displacement are 1 mm lower than those shown in the diagrams on Fig. 8 due to the one-millimeter free travel of the testing machine traverse. The coefficient of variation (CoV – standard deviation/mean value multiplied by 100%) for the maximum force was 1.30%, indicating very low variability among the tested BCC specimens. In comparison, the displacement exhibited a higher CoV of 6.76% and 12.34%, indicating greater specimen-to-specimen variability in deformation at the maximum force and total displacement due manufacturing defects in test samples, which requires further investigation. The force and displacement values throughout the experimental test were extracted and subsequently transferred to graphs that will serve as the basis for calculating the energy absorption capacity. Figs. 9 – 12 show the course of the compression test BCC test specimens with the indicated percentage of deformation lattice structures during compression.

Table 2. Values of maximum forces before the first significant lattice structures fracture with corresponding displacement and total displacement

Sample	Maximum force (N)	Displacement for maximum force (mm)	Total displacement (mm)
BCC – 1	2554.19	3.99	7.65
BCC – 2	2556.29	4.09	6.86
BCC – 3	2486.50	4.36	9.10
BCC – 4	2522.60	3.70	7.40
Mean value	2529.89	4.04	7.75
St. deviation	32.78	0.27	0.96
CoV	1.30%	6.76%	12.34%

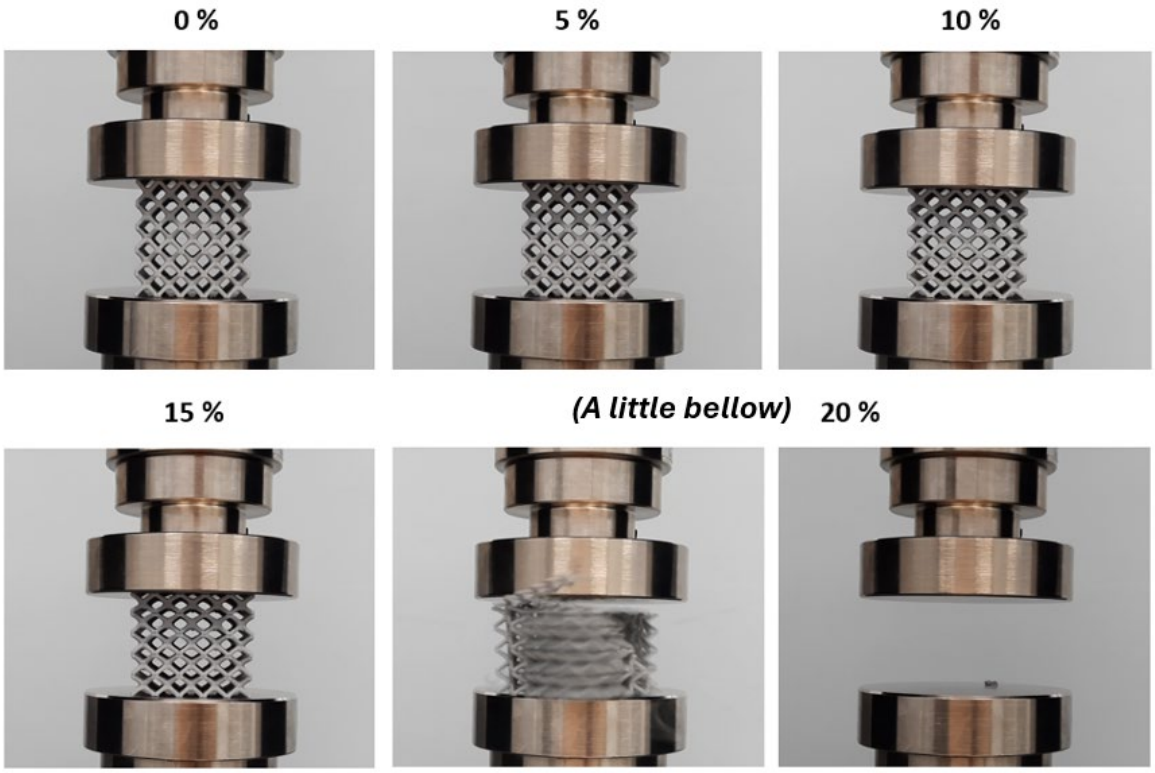


Fig. 9. Compression fracture of sample BCC – 1 with compressive deformation until complete failure of the lattice structure

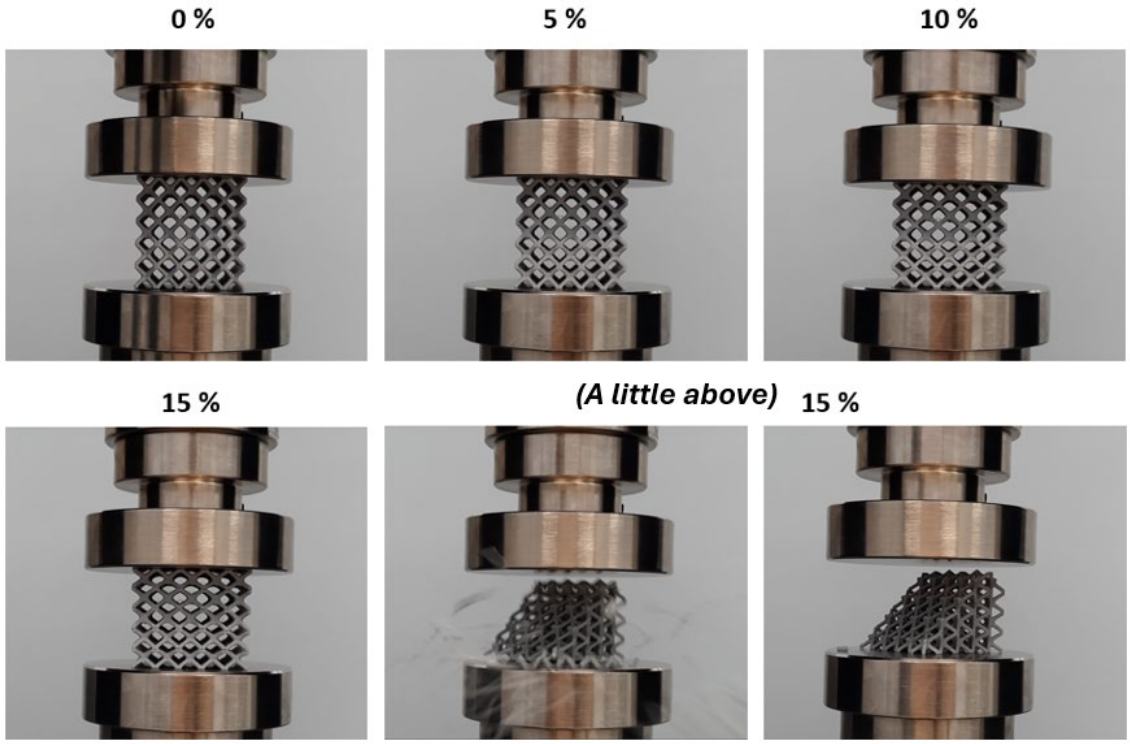


Fig. 10. Compression fracture of sample BCC – 2 with compressive deformation until complete failure of the lattice structure

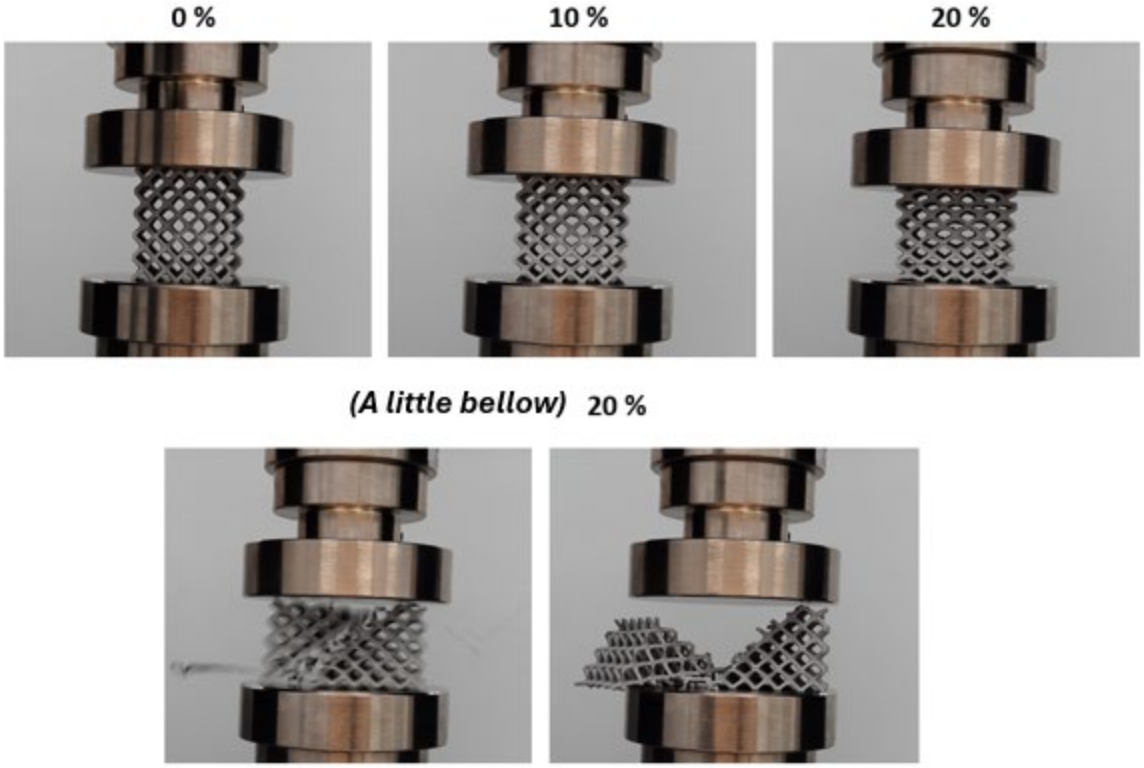


Fig. 11. Compression fracture of sample BCC – 3 with compressive deformation until complete failure of the lattice structure

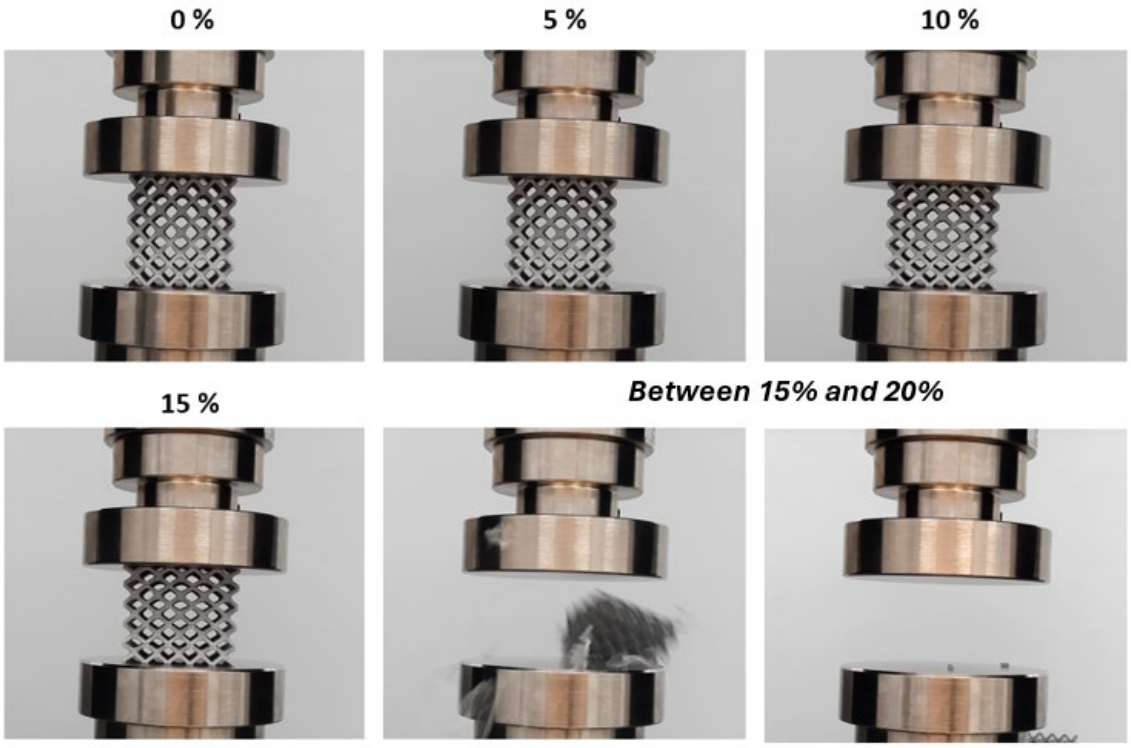


Fig. 12. Compression fracture of sample BCC – 4 with compressive deformation until complete failure of the lattice structure

7. Compression Test Results Validation

7.1 Intuitive Interpretation of The Compression Test Results

In all test specimens, as shown in Figs. 9 – 12, in the initial loading phase, an almost uniform elastic behavior of the lattice structures is visible without significant instabilities. This indicates that in the initial elastic phase, the structures evenly distribute the external compression load over the unit cells of the BCC lattice structure, as confirmed by the diagram shown in Fig. 8. Increasing the deformation leads to a stress concentration in the middle part of the lattice structure, which is absorbed by the lateral bending of the test specimen and leads to a balloon-like shape of the test specimen (visible in Figs. 9, 10 and 12 at around 15% compressive deformation of the specimen and Fig. 11 at around 20% compressive deformation of the specimen). The reason for these lies precisely in the topology of the BCC unit cell by which the struts are stretched during compression testing. That indicates that the Maxwell criterion mentioned earlier in Eq. (3) is not reliable for determining the compression behavior of a BCC lattice structure with a circular cross-section of unit cells made of PLA material FFF additive manufacturing process, with this chosen unit cell dimension, multiplication pattern and lattice structure final dimension. Furthermore, a comparison of the force – displacement response presented in Fig. 8 with the conventional stress – strain behavior, reported early in text in Fig. 2 for bending-dominated lattice structures, reveals the absence of a distinct and uniform collapse region during compression. Instead, the structure exhibits a parabolic, knee-shaped response with a pronounced peak in the load-bearing capacity, corresponding to the dominant collapse stage of the lattice structure. After reaching the maximum force, the unit cells suddenly stretch, yield, and the final loss of stability of the entire lattice structure occurs – a fracture along the diagonal of the lattice structure, which is visible at the end of all samples in this compression test. The diagonal fracture observed in the BCC lattice specimens can be attributed to the characteristic deformation mechanism of BCC topologies under compressive loading, as shown on Figs. 13 and 14. The BCC topology is characterized by diagonal struts connecting the center of the unit cell. Under compressive loading, the applied load is primarily transferred through these struts. However, their deformation is not purely axial. Due to their relatively high slenderness, additive manufacturing defects, load eccentricities and local

stress concentrations, the struts are susceptible to bending, stretching and buckling. Once local buckling occurs, the applied load is redistributed to the adjacent struts, promoting progressive deformation and failure within the lattice structure. This process leads to the development and propagation of a localized deformation zone along the diagonal of the BCC structure.

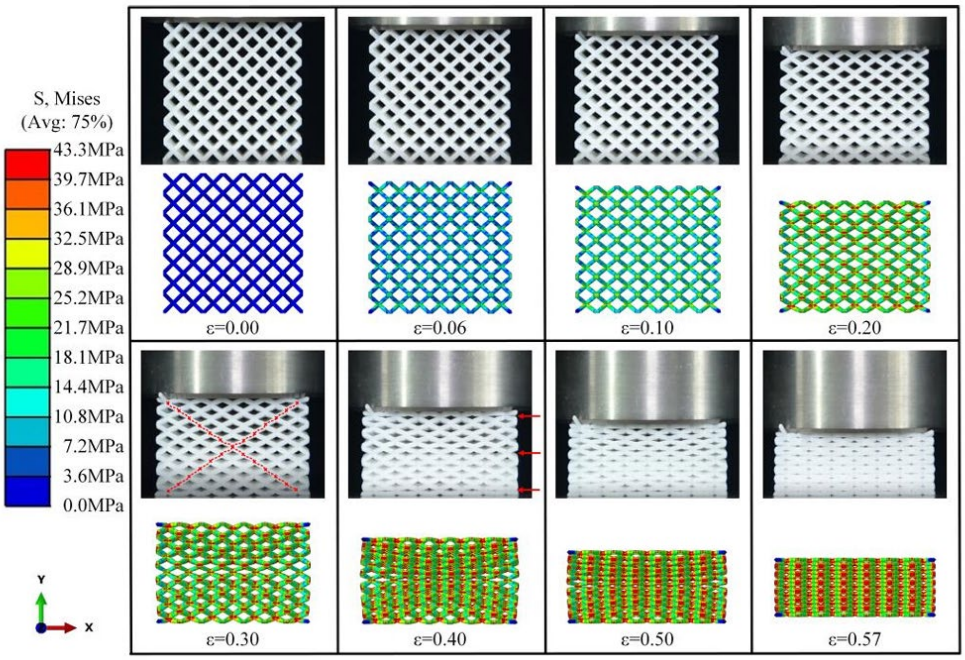


Fig. 13. Deformation during compression test of BCC uniform lattice structure (experimental test and simulation) [22]

Previous studies have reported the formation of diagonal shear bands, typically oriented at approximately 45° to the loading direction, because of progressive buckling and failure of individual struts. The initial buckling of struts locally reduces the load-bearing cross-section, promoting stress redistribution to adjacent struts and resulting in the progressive propagation of the failure zone along the diagonal direction [22-24]. In the present study, however, the deformation mechanism was strongly influenced by the brittle behavior of the PLA material used for specimen fabrication. Unlike ductile metallic BCC lattices, as presented in [23], in which strut buckling can be accompanied by progressive plastic deformation and gradual collapse, the limited plastic deformation capacity of PLA promotes crack initiation at highly stressed or locally buckled struts, followed by rapid crack propagation through the lattice. Consequently, the characteristic diagonal deformation band developed into a sudden diagonal fracture of the specimens rather than a gradual progressive collapse. This suggests that the observed failure mode results from the combined effect of the intrinsic deformation mechanism of the BCC topology and the limited fracture resistance of the PLA material.

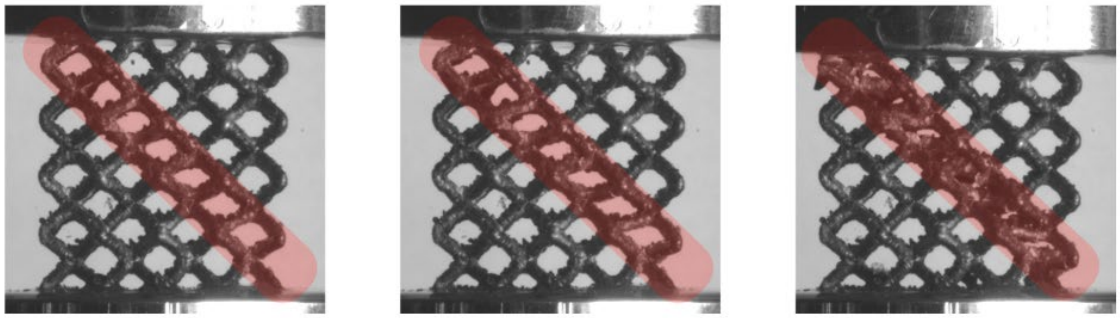


Fig. 14. Diagonal shear band in metallic BCC lattice sample [25]

The differences between the samples are primarily manifested in the moment of the first instability, and the ability to absorb energy before complete fracture. This is evident in Fig. 8 due to the different displacement values observed for the individual specimens. Since all test samples fracture

equally along the diagonal of the lattice structure, the relatively rigid behavior of the PLA BCC lattice structure, high initial load capacity but reduced ability to absorb energy after the initial fracture is concluded since the complete fracture of the lattice structure occurs at relatively small deformations of the test samples (Figs. 9 – 12 between 15% and 20%). This behavior may be attributed to imperfections introduced during the FFF additive fabrication of the specimens, as well as to interlayer defects and discontinuities resulting from the layer-by-layer manufacturing process. An increase in the energy absorption capacity could be achieved by extending the duration of the compression test of the test specimen without such a sudden failure of the lattice structure.

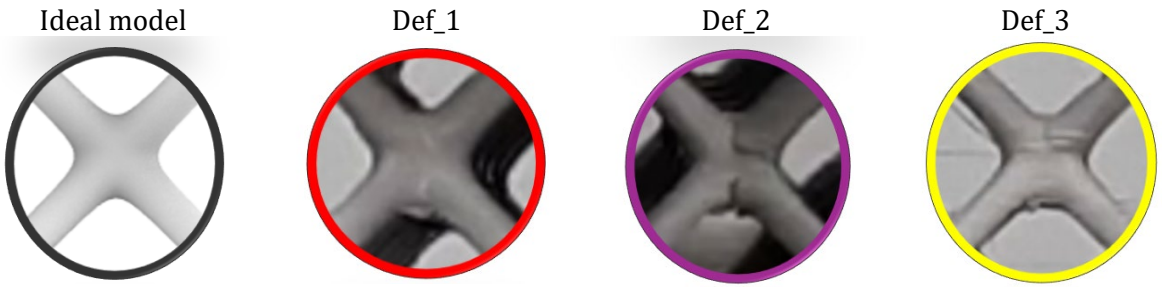


Fig. 15. Physically visible dominant manufacturing defects in tests specimens

Fig. 15 summarizes three defects identified during the FFF additive manufacturing process. Defect 1 (Def_1) resulted from the action of gravitational forces on the deposited molten layer. This is manifested by the formation of folds on the underside of the unit cell central node. Defect 2 (Def_2) was attributed to stresses generated during layer solidification and manifested as a visible crack. Defect 3 (Def_3) resulted from a combination of Def_1 and Def_2. Each of these manufacturing defects was assigned a specific color for identification and was detected exclusively in the frontal plane of the specimens during the compression test, as shown in Fig. 16. The identified defects were quantified and their influence on the compressive test results was investigated, as this parameter is directly related to the specific energy absorption of the lattice structures due to its influence on the specimen mass and duration of the compression test (i.e., the deformation of the specimens). Following the detection of defects in the frontal plane of the test specimens, it was concluded that BCC – 1 and BCC – 4 exhibited predominantly gravity-induced defects at the nodes, resulting from the deformation of the deposited molten material, whereas BCC – 2 and BCC – 3 exhibited predominantly node cracking caused by residual stresses generated during layer solidification.

7.2. Quantitative Interpretation of Compression Results

The results of the experimental compression testing of PLA BCC lattice structures show a relatively uniform mechanical behaviors of all tested samples in terms of achieving the maximum force, which indicates good repeatability of the 3D printing process and uniform behavior of the unit cell topology itself during compression testing. The values of the maximum force during compression load range from approximately 2486.5 N to 2556.29 N, as stated at Table 2. The difference between the highest and lowest measured forces is about 70 N which indicates a small dispersion and very good homogeneity of the results. The error bars, shown at Fig. 17, reveal relatively low scatter in the maximum force and CoV of 1.3% (shown at Table 2) indicating good consistency in the load-bearing capacity of the BCC specimens. Greater dispersion is observed for the displacement parameters, particularly the total displacement (7.75 ± 0.96 mm; CoV=12.34%), shown at Fig. 17 and Table 2, suggesting greater specimen-to-specimen variability due to manufacturing defects associated with additive manufacturing, particularly in terms of deformation and collapse behavior.

The obtained values of the work of external force, i.e. the ability of the samples to absorb energy for the tested samples are in the range from 12.50 J to 16.30 J (as shown in Figure 18) with a mean value of approximately 14.14 J and a standard deviation of 1.60 J, as shown on Table 3. The coefficient of variation is 11.32%, which indicates a moderate dispersion of the results. Dispersion in the results is expected, especially in materials obtained by additive technologies or in complex lattice structures, where local geometric irregularities significantly affect the mechanical response.

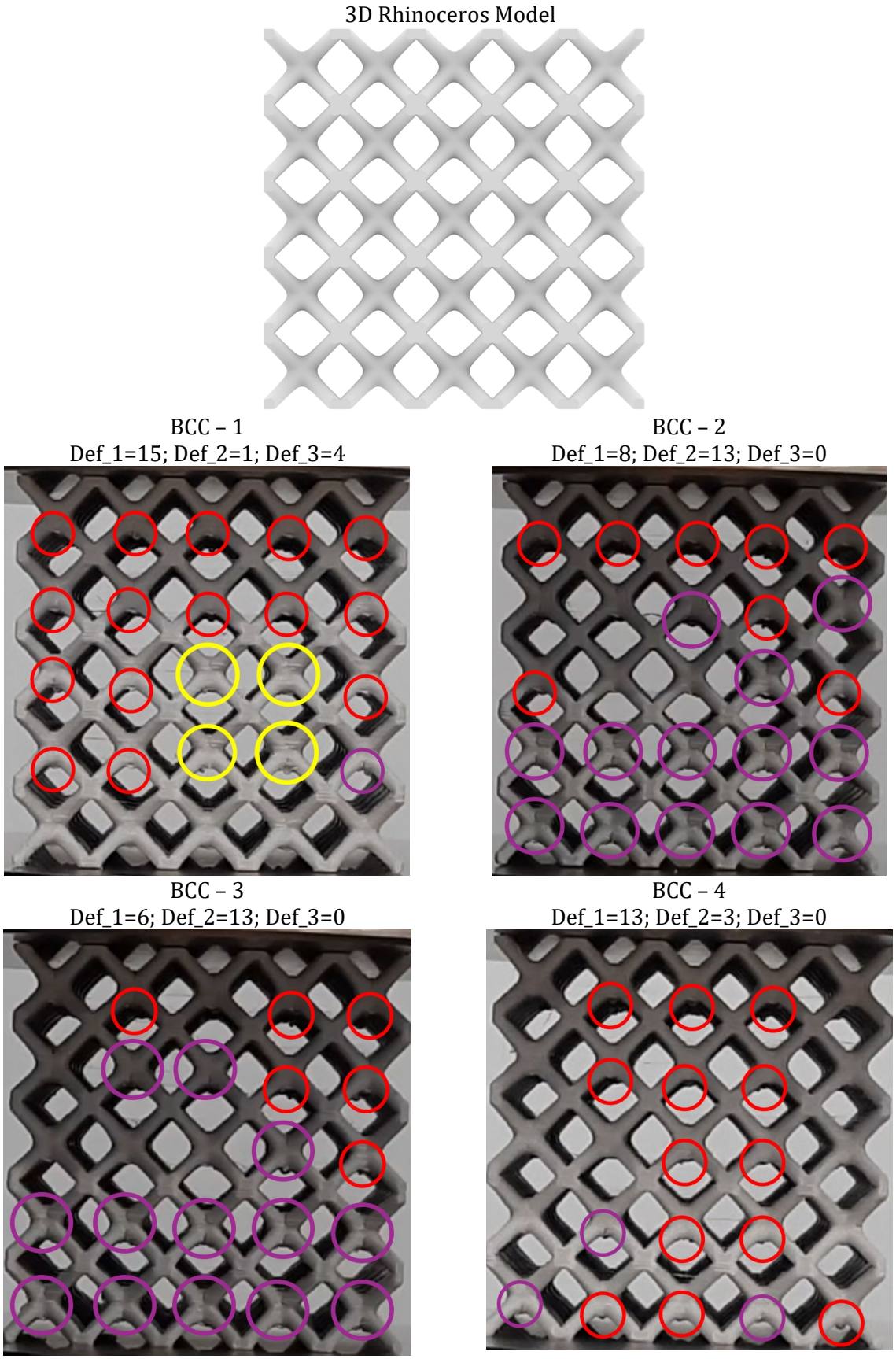


Fig. 16. Significant manufacturing defects detected in the lattice test specimens

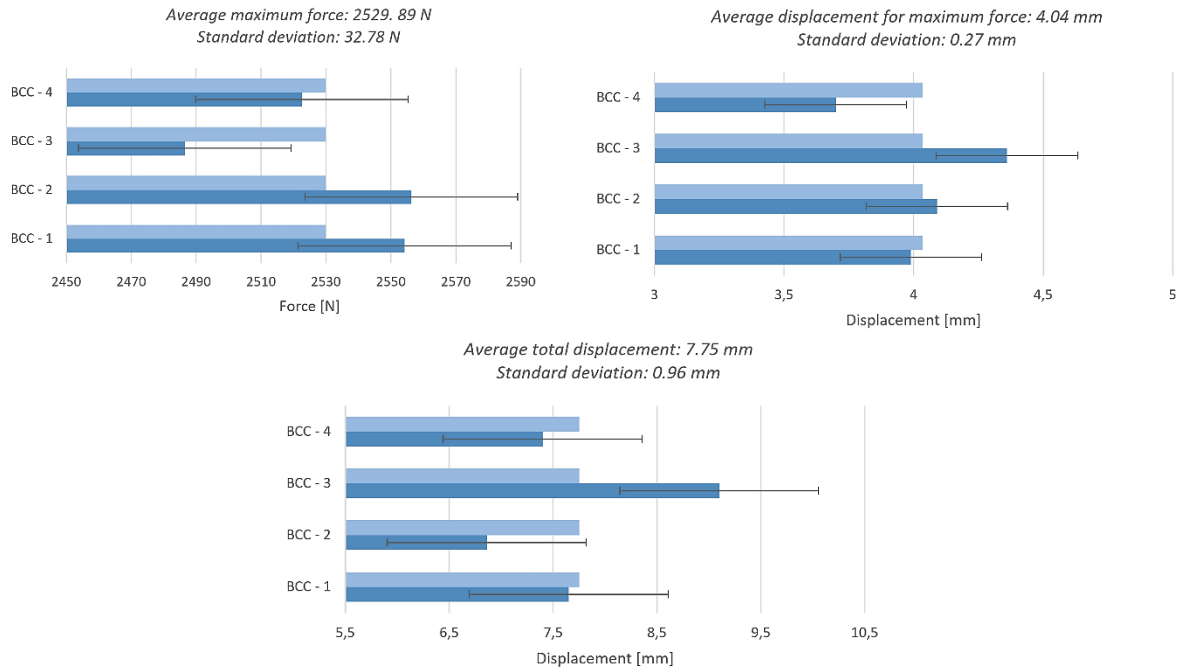


Fig. 17. Graphs of average maximum force (top left), average displacement for maximum force (top right) and average total displacement (bottom) with standard deviation and error bars for each lattice specimen

Table 3. Energy absorption EA, sample mass and specific energy absorption SEA

Sample	Energy Absorption EA (J)	Sample mass m (g)	Specific Energy Absorption SEA (J/g)
BCC – 1	14.22	34.94	0.41
BCC – 2	12.50	34.90	0.36
BCC – 3	16.30	34.92	0.47
BCC – 4	13.55	34.87	0.39
Mean value	14.14	34.91	0.41
St. deviation	1.60	0.03	0.05
CoV	11.32%	0.09%	11.32%

The energy absorption results indicate that the manufacturing-induced defects identified in the BCC lattice structures investigated contributed to the specimen-to-specimen variation in mechanical response, as shown in Fig. 19. The mean energy absorption (EA) was 14.14 ± 1.60 J, while the corresponding specific energy absorption (SEA) was 0.41 ± 0.05 J/g, resulting in identical coefficients of variation of 11.32% as shown on Table 3. In contrast, the sample mass exhibited an extremely low variation (34.91 ± 0.03 g; CoV = 0.09%), indicating that the observed differences in SEA were not associated with variations in specimen mass, but were primarily related to differences in structural response, which can be attributed to manufacturing defects. This is consistent with previous studies showing that manufacturing imperfections can cause deviations from the nominal CAD geometry and modify the mechanical response and failure behaviors of additively manufactured lattice structures under compression [26]. Such variations are also expected to influence the load-transfer mechanisms and energy-absorption performance of the lattice structure. In the present study, BCC – 1 exhibited the highest number of Def_1 defects (15), associated with the deformation of the deposited molten material under gravitational forces, together with four Def_3 defects and one Def_2 defect, as shown on Figure 16. SEA of 0.41 J/g for BCC – 1 corresponds to the overall mean value. This suggests that Def_1 type imperfections, although numerous, did not necessarily act as critical fracture initiation sites. Instead, such defects may primarily introduce local geometric deviations and changes in strut stiffness, allowing the structure to retain a considerable capacity for progressive deformation and energy absorption.

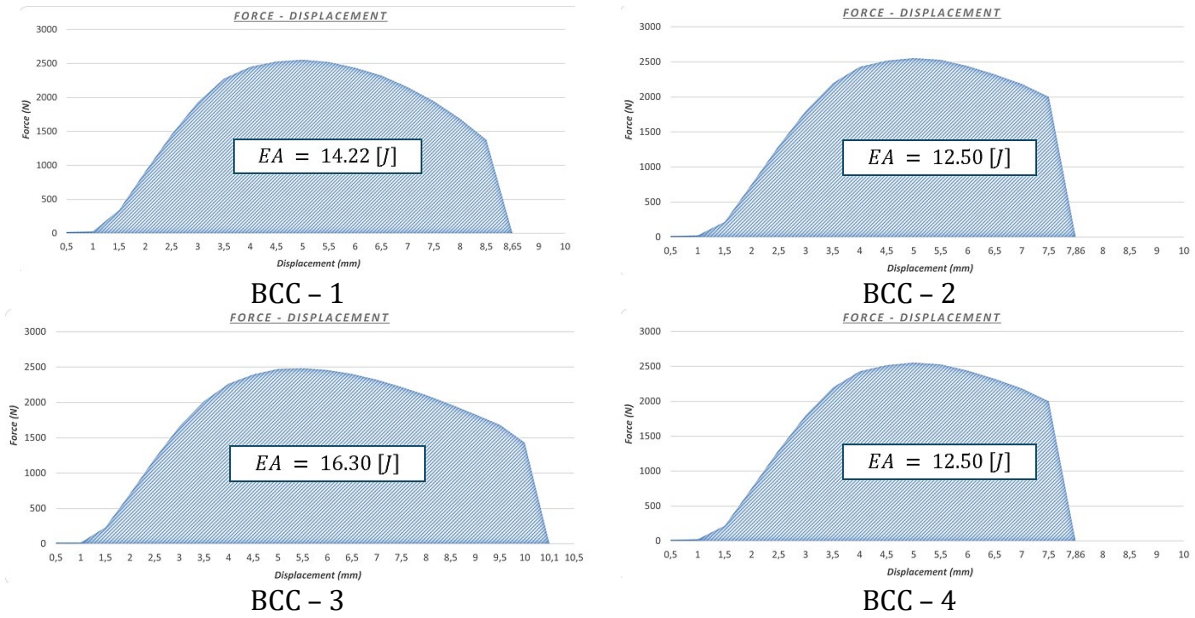


Fig. 18. The area under the force – displacement diagram represents the work of the external force, i.e. the total energy absorbed by the sample during loading

The relatively moderate influence of these imperfections is further supported by the performance of BCC – 4, which contained 13 Def_1 defects and only three Def_2 defects, as shown on Fig. 16 and exhibited an intermediate SEA of 0.39 J/g. A more pronounced reduction in energy absorption was observed for BCC – 2, which exhibited 13 Def_2 defects associated with solidification-induced stresses and visible cracking, as shown on Fig. 16. This specimen recorded the lowest EA (12.50 J) and SEA (0.36 J/g), approximately 11.6% below the mean SEA. Unlike Def_1, which primarily represents a geometric imperfection caused by deformation of the molten deposited material, Def_2 represents a material discontinuity that can act as a local stress concentrator and facilitate premature failure of the load-bearing struts. Such behavior is particularly relevant for BCC architectures because the inclined struts and their connecting nodes constitute preferential load-transfer paths and regions of stress concentration. Previous investigations of polymeric BCC lattices have demonstrated that manufacturing-induced defects should be considered when accurately reproducing their compressive response, while the morphology and spatial distribution of defects, particularly within struts and nodal regions, can significantly affect local stress concentrations, deformation and failure behaviors [27]. The present results therefore suggest that crack-type Def_2 imperfections may have a greater detrimental effect on energy absorption than Def_1 imperfections when they intersect or occur close to critical load-bearing regions. However, this interpretation should not be reduced to a simple relationship between defect number and energy absorption. BCC – 3 contained the same number of Def_2 defects as BCC – 2 (13 defects), as shown on Figure 16, yet exhibited the highest EA (16.30 J) and SEA (0.47 J/g), with the latter being approximately 15.2% higher than the mean value and 30.3% higher than that of BCC – 2. This finding demonstrates that the absolute number of defects is insufficient to explain the energy-absorption behavior of the investigated structures. The contrasting responses of BCC – 2 and BCC – 3 indicate that the mechanical significance of a manufacturing defect is governed not only by its type and frequency, but also by its spatial distribution, size, orientation and interaction with the principal load-bearing members. In BCC – 3, the lower number of Def_1 imperfections compared with BCC – 2, together with the specific spatial arrangement of the observed Def_2 defects, may have allowed the structure to maintain more effective load transfer between the BCC struts and undergo greater deformation before catastrophic failure. Consequently, the higher SEA of BCC – 3 should not be interpreted as evidence that Def_2 defects improve energy absorption, rather, it highlights the stochastic nature of defect distribution and its interaction with the lattice architecture. This interpretation is consistent with previous research showing that the effect of additive-manufacturing defects on the mechanical and energy-absorption performance of lattice structures depends not only on defect population, but also on defect type, morphology, severity and spatial distribution [28].

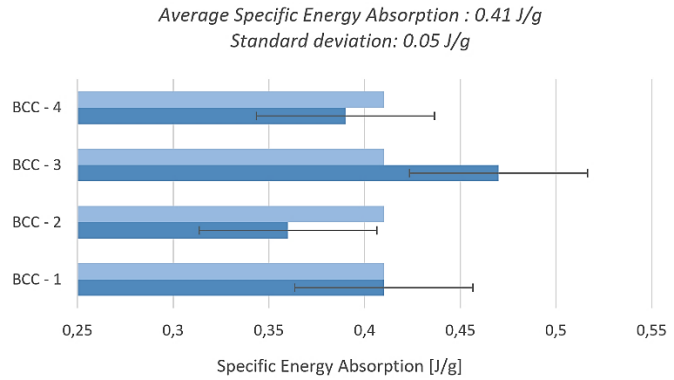


Fig. 19. Average specific energy absorption (SEA) with standard deviations and error bars for all tests specimens

Overall, the present results demonstrate that the FFF-produced BCC PLA lattice structure should be assessed not simply by counting visible defects, but by considering their mechanical relevance to the load-bearing architecture. The relatively low mass variation and moderate CoV of EA and SEA indicate that the investigated structures exhibit generally consistent energy-absorption behaviour, while the differences between individual specimens demonstrate that localized manufacturing imperfections can govern the onset and progression of failure. The defects observed in the FFF printed lattice structures were identified through visual inspection of the specimens. Although this approach enabled the identification and qualitative description of visible printing imperfections, a more detailed characterization of the defect morphology and their potential influence on failure mechanisms would require microscopic analysis. Scanning electron microscopy (SEM) could provide further insight into fracture surface morphology, interlayer adhesion, porosity and localized defects at the strut and node regions, helping to elucidate their influence on the energy absorption capability of the lattice structures. Such analysis was beyond the scope of the present study and is therefore considered a subject for future work. Based on the conducted tests, it can be concluded that the analyzed PLA BCC lattice structures show satisfactory potential for applications in which effective energy absorption capacity for small deformations of the structure and with a relatively small mass associated with a low relative density (in this case of approximately 0.2) is important, such as protective elements and elements used for energy absorption purposes (e.g. in the automotive industry).

8. Conclusions

In this research, the compressive properties and energy absorption capacity of BCC lattice structures manufactured by FFF 3D printing technology using PLA material were experimentally tested. The lattice structures were modelled in the Rhinoceros program, with the Grasshopper plugin, with a relative density of approximately 0.2 and were subjected to compression testing on Shimadzu AGS-X 100 kN universal testing machine. The experimental results demonstrate a generally consistent initial mechanical response of the investigated PLA BCC lattice structures, as evidenced by the low dispersion in the maximum compressive force (CoV=1.30%). However, greater variability was observed in the displacement and energy-absorption parameters, with the total displacement showing a CoV of 12.34% and both EA and SEA exhibiting a CoV of 11.32%. This indicates that, although the load-bearing capacity of the specimens was highly repeatable, the deformation and energy-absorption behavior was more sensitive to specimen-to-specimen variations. The observed deformation behavior was characterized by an initially uniform elastic response followed by localized deformation, lateral bending and progressive instability of the BCC struts. The subsequent development of a diagonal failure zone and sudden fracture can be attributed to the combined influence of the inherent deformation mechanism of the BCC topology, local buckling, manufacturing defects and stress concentration and the relatively brittle behavior of PLA. Consequently, the investigated structures did not exhibit a pronounced and uniform post-yield collapse plateau characteristic of ductile or bending-dominated cellular structures, but rather a pronounced peak load followed by rapid loss of structural stability at relatively small compressive deformations. The identified manufacturing-induced defects further contributed to the variability

of the energy-absorption response. In particular, the comparison between BCC – 2 and BCC – 3 demonstrates that defect number alone is insufficient to predict the mechanical performance of the lattice structures. Despite containing the same number of Def_2 defects, BCC – 2 exhibited the lowest SEA (0.36 J/g), whereas BCC – 3 achieved the highest value (0.47 J/g), highlighting the stochastic interaction between manufacturing imperfections and lattice topology. Overall, the investigated PLA BCC lattice structures demonstrated satisfactory energy-absorption potential for applications requiring lightweight structures and energy dissipation over relatively small deformation ranges. The low variation in specimen mass (CoV = 0.09%) confirms that the observed differences in SEA primarily originated from variations in structural deformation and failure behavior due to manufacturing irregularities. Diagonal fracture and limited deformation capacity indicate that further optimization of the lattice geometry, manufacturing parameters and defect control is required to increase the deformation range and promote more progressive energy absorption. Such improvements could enhance the suitability of PLA BCC lattice structures for lightweight protective and energy-absorbing components, including potential applications in the automotive sector. Therefore, future investigations should combine defect quantification with their spatial location and geometric characteristics, preferably using techniques such as micro-computed tomography or high-resolution microscopy, to establish a quantitative relationship between defect morphology, failure initiation and energy-absorption performance. SEM-based characterization could provide further insight into the relationship between printing defects, fracture behavior and the energy absorption capability of the investigated lattice structures. A limitation of the present study is the relatively small number of tested specimens (n = 4). Accordingly, the statistical evaluation was limited to descriptive statistics and the reported variability should be interpreted in this context. Further studies involving a larger number of specimens are recommended to provide more robust statistical validation of the observed trends.

References

[1] Intrigila C, Nodargi NA, Bisegna P. The compressive response of additively-manufactured hollow truss lattices: an experimental investigation. International Journal of Advanced Manufacturing Technology. 2022 May 1;120(5-6):3529-41. https://doi.org/10.1007/s00170-022-08716-0

[2] Alhembar A, Sheikh-Ahmad J, Jarrar F, Bojanampati S. Optimizing the specific mechanical properties of lattice structures fabricated by material extrusion additive manufacturing. Journal of Materials Research and Technology. 2023 Jan 1; 22:1821-38. https://doi.org/10.1016/j.jmrt.2022.12.024

[3] Zhang J, Huang H, Liu G, Zong H, Zhang C. Stiffness and energy absorption of additive manufactured hybrid lattice structures. Virtual Phys Prototyp. 2021;16(4):428-43. https://doi.org/10.1080/17452759.2021.1954405

[4] Park KM, Min KS, Roh YS. Design Optimization of Lattice Structures under Compression: Study of Unit Cell Types and Cell Arrangements. Materials. 2022 Jan 1;15(1). https://doi.org/10.3390/ma15010097

[5] Niutta CB, Ciardiello R, Tridello A. Experimental and Numerical Investigation of a Lattice Structure for Energy Absorption: Application to the Design of an Automotive Crash Absorber. Polymers (Basel). 2022 Mar 1;14(6). https://doi.org/10.3390/polym14061116

[6] Bustihan A, Botiz I. Recent Advances in Additively Manufactured Polymeric Structures for Mechanical Energy Absorption. Polymers. Multidisciplinary Digital Publishing Institute (MDPI); 2026. https://doi.org/10.3390/polym18091019

[7] Bieler S, Weinberg K. Energy absorption of sustainable lattice structures under static compression. Meccanica. 2025 Aug 1;60(8):2533-47. https://doi.org/10.1007/s11012-025-02003-4

[8] Banaszek M, Baranowski P, Płatek P, Sarzyński M, Cieplak K. Studies of energy absorption of lattice structures manufactured from PETG filament with FFF 3D printing. Bulletin of the Polish Academy of Sciences Technical Sciences. 2025 Sep 1;155047-155047. https://doi.org/10.24425/bpasts.2025.155047

[9] Kumar A, Verma S, Jeng JY. Supportless lattice structures for energy absorption fabricated by fused deposition modeling. 3D Print Addit Manuf. 2020 Apr 1;7(2):85-96. https://doi.org/10.1089/3dp.2019.0089

[10] Azmi MS, Ismail R, Hasan R. Investigation on the static and dynamic behavior of BCC lattice structure with quatrefoil node manufactured using fused deposition modelling additive manufacturing. In: IOP Conference Series: Materials Science and Engineering. Institute of Physics Publishing; 2020. https://doi.org/10.1088/1757-899X/788/1/012008

[11] Distefano F, Guglielmino E, Mineo R, Epasto G. Mechanical and morphological characterization of BCC - Derived unit cells for biomedical devices. In: Procedia Structural Integrity. Elsevier B.V.; 2022. p. 470-85. https://doi.org/10.1016/j.prostr.2022.05.053
[12] Dong P, Ding W, Yuan H, Wang Q. 3D-printed polymeric lattice-enhanced sustainable municipal solid waste incineration fly ash alkali-activated cementitious composites. Developments in the Built Environment. 2022 Dec 1;12. https://doi.org/10.1016/j.dibe.2022.100101
[13] Yu Z, Savinov R, Matura M, Zhang P, Shi J. Current research status on advanced lattice structures for impact and energy absorption applications: A systematic review. Thin-Walled Structures. Elsevier Ltd; 2025. https://doi.org/10.1016/j.tws.2025.113490
[14] Xu C, Daynes S, Das R, Kabaliuk N. Anisotropic mechanical properties and energy absorption of TPMS structures: a comparative study of polylactic acid and thermoplastic polyurethane materials. Thin-Walled Structures. 2025 Dec 1;217. https://doi.org/10.1016/j.tws.2025.113868
[15] Yin H, Zhang W, Zhu L, Meng F, Liu J, Wen G. Review on lattice structures for energy absorption properties. Compos Struct. 2023;304(P1):116397. https://doi.org/10.1016/j.compstruct.2022.116397
[16] Benedetti M, du Plessis A, Ritchie RO, Dallago M, Razavi N, Berto F. Architected cellular materials: A review on their mechanical properties towards fatigue-tolerant design and fabrication. Materials Science and Engineering R: Reports. 2021; 144:100606. https://doi.org/10.1016/j.mser.2021.100606
[17] Li Y, Jiang D, Zhao R, Wang X, Wang L, Zhang LC. High Mechanical Performance of Lattice Structures Fabricated by Additive Manufacturing. Metals. Multidisciplinary Digital Publishing Institute (MDPI); 2024. https://doi.org/10.3390/met14101165
[18] Ghaemi Khiavi S, Mohammad Sadeghi B, Divandari M. Effect of topology on strength and energy absorption of PA12 non-auxetic strut-based lattice structures. Journal of Materials Research and Technology. 2022; 21:1595-613. https://doi.org/10.1016/j.jmrt.2022.09.116
[19] Baddour M, Fiorillo C, Trossaert L, Verberckmoes A, Ghekiere A, D'hooge DR, et al. Comparing Degradation Mechanisms, Quality, and Energy Usage for Pellet- and Filament-Based Material Extrusion for Short Carbon Fiber-Reinforced Composites with Recycled Polymer Matrices. Journal of Composites Science. 2024 Jun 1;8(6). https://doi.org/10.3390/jcs8060222
[20] Suksawang B, Chaijareenont P, Silthampitag P. Effect of Unit Cell Design and Volume Fraction of 3D-Printed Lattice Structures on Compressive Response and Orthopedics Screw Pullout Strength. Materials. 2025 Mar 1;18(6). https://doi.org/10.3390/ma18061349
[21] Intrigila C, Nodargi NA, Bisegna P. The compressive response of additively-manufactured hollow truss lattices: an experimental investigation. International Journal of Advanced Manufacturing Technology. 2022 May 1;120(5-6):3529-41. https://doi.org/10.1007/s00170-022-08716-0
[22] Bai L, Gong C, Chen X, Sun Y, Xin L, Pu H, et al. Mechanical properties and energy absorption capabilities of functionally graded lattice structures: Experiments and simulations.
[23] Frasch J, von Lukowicz H, Risse S. Investigation of additively manufactured lattice structures for refractive optical systems based on auxetic properties. Progress in Additive Manufacturing. 2024 Jun 1;9(3):655-64. https://doi.org/10.1007/s40964-024-00658-1
[24] Yang Y, Shan M, Zhao L, Qi D, Zhang J. Multiple strut-deformation patterns based analytical elastic modulus of sandwich BCC lattices. Mater Des. 2019 Nov 5;181. https://doi.org/10.1016/j.matdes.2019.107916
[25] Ho NSK, Chai GB, Li P. Fracture behaviour of laser powder bed fusion AlSi10Mg microlattice structures under uniaxial compression. Mater Des. 2023 Dec 1;236. https://doi.org/10.1016/j.matdes.2023.112489
[26] Amirpour M, Battley M. Study of manufacturing defects on compressive deformation of 3D-printed polymeric lattices. International Journal of Advanced Manufacturing Technology. 2022 Sep 1;122(5-6):2561-76. https://doi.org/10.1007/s00170-022-10062-0
[27] Bruson D, Serrano-Munoz I, Fritsch T, Markötter H, Galati M. Revealing the (positive) role of porosity within polymeric additively manufactured lattices via X-ray computed tomography. Int J Solids Struct. 2025 Sep 1;320. https://doi.org/10.1016/j.ijsolstr.2025.113488
[28] Boursier Niutta C, Ciardiello R, Berto F, Paolino DS, Tridello A. On the influence of Additive Manufacturing defects on the energy absorption capability of a lattice structure. In: Procedia Structural Integrity. Elsevier B.V.; 2022. p. 1449-57. https://doi.org/10.1016/j.prostr.2022.12.185